

Ion-Track Modification of a Silicon-Dioxide Film Implanted with Zinc Ions and Annealed in Oxygen

V. V. Privezentsev^{a, b, *}, A. N. Palagushkin^b, V. A. Skuratov^c, V. S. Kulikauskas^d, V. V. Zatekin^d,
A. V. Makunin^d, D. A. Kiselev^e, E. A. Steinman^f, and A. N. Tereshchenko^f

^aInstitute of Physics and Technology, Russian Academy of Sciences, Moscow, 117218 Russia

^bResearch Institute for System Studies, Russian Academy of Sciences, Moscow, 117218 Russia

^cJoint Institute for Nuclear Research, Dubna, Moscow Oblast, 141980 Russia

^dSkobel'syn Research Institute of Nuclear Physics, Moscow State University, Moscow, 119991 Russia

^eNational Research University of Science and Technology MISiS, Moscow, 119049 Russia

^fInstitute of Solid-State Physics, Russian Academy of Sciences, Chernogolovka, Moscow oblast, 142432 Russia

*e-mail: v.privezentsev@mail.ru

Received June 28, 2018; revised July 21, 2018; accepted July 25, 2018

Abstract—The formation of a zinc-oxide phase in a SiO₂ film deposited onto *n*-type Si substrates grown in the (100) orientation using the Czochralski technique, which is a result of implanting ⁶⁴Zn⁺ ions at room temperature, an energy of 50 keV, and a dose of 5×10^{16} cm⁻², and subsequent heat treatment in an oxygen atmosphere at elevated temperatures, is studied. The surface topology is investigated using methods of scanning electron and atomic force microscopy. The optical properties are studied using the method of photoluminescence spectroscopy at 10 K and by measuring the light reflection spectra. After Zn implantation, a ZnO phase is detected in the subsurface layer of the SiO₂ film. After low-temperature annealing in the range of 400–600°C, Zn-containing precipitates with a cross-sectional size of particles of 20–50 nm are found in the sample and on its surface. After annealing at 700–800°C, Zn-containing precipitates of the Zn·ZnO complex are formed in the subsurface layer, and a phase of the ZnO·Zn₂SiO₄ complex is found after annealing at temperatures of 900–1000°C. The samples obtained at the annealing temperature optimal for the formation of the ZnO phase (about 700°C) are irradiated with ¹³²Xe²⁶⁺ ions with an energy of 167 MeV. The ZnO phase is found to disappear after irradiation at a fluence of 2×10^{13} cm⁻² and a large number of radiation-induced defects giving a characteristic photoluminescence band are formed. With an increase in the Xe fluence to 5×10^{14} cm⁻², the intensity of this luminescence band increases.

Keywords: silicon-oxide film, zinc implantation, Zn-containing precipitates, irradiation with fast heavy ions

DOI: 10.1134/S102745101902037X

INTRODUCTION

Recently, the properties of nanoparticles of metals and their oxides in various light-transmitting dielectric matrices have been widely studied, since such nanostructured materials are very different in their properties from bulk materials similar in composition and can be used in promising opto-, nano-, and microelectronics devices [1]. The method of ion doping is most suitable for the formation of such nanoparticles, since it has important features, such as: a purity of materials to a level of 99.999% due to mass separation; the possibility of choosing the implanted element and implantation doses; and other advantages. The main advantage of this method is that it can be used to obtain concentrations of implanted metal dopants far above the limit of their equilibrium solubility in the substrate. In this method, heat treatment is used not

only for annealing radiation-induced defects, but also for the nucleation and growth of metal and metal-oxide nanoparticles [2]. Therefore, studies of dielectric films doped with metal impurities, in particular, zinc, have become very important and are carried out quite intensively [3–5].

Among metal-oxide materials, zinc oxide should be noted, since ZnO is a direct-gap material with a bandgap of 3.37 eV and it has a large electron–hole binding energy of 60 meV in an exciton, which makes it possible to obtain UV radiation with a wavelength of $\lambda = 390$ nm at temperatures up to 350°C. Therefore, matrices with ZnO nanoparticles can be widely used in modern optoelectronic devices, such as UV lasers and LEDs [6], and electroluminescent displays [7]. Their application is promising in solar cells [8], as well as in gas-sensor devices [9]. Recently, after the discovery of

room-temperature ferromagnetism in structured zinc-oxide films, the question arose whether such a material could be used in spintronics devices [10]. The possibility of using zinc-oxide films or ZnO precipitates in polymer matrices to create non-volatile memory devices is currently being discussed [11].

Zinc-oxide nanoparticles in a SiO₂ film can be formed during heat treatment in an oxidizing atmosphere of zinc precipitates preliminarily created in a silicon-oxide film doped with Zn ions [12–14]. As noted above, extremely large concentrations of zinc ions (up to 25 at %) can be obtained with the incorporation of this element into the silicon-oxide film [15].

In this work, the conditions for the formation of zinc-oxide nanoparticles in a SiO₂ film thermally grown on an *n*-type silicon substrate with the (100) orientation obtained by the Czochralski method are studied.

MATERIALS AND METHODS

First, a 0.2- μm -thick SiO₂ film was obtained in a dry oxygen atmosphere at a temperature of 700°C on an *n*-type silicon substrate grown in the (100) orientation by the Czochralski method. Then, ⁶⁴Zn⁺ ions were implanted at room temperature, an energy of 50 keV, and a dose of $5 \times 10^{16} \text{ cm}^{-2}$. The ion current was maintained at 0.55 $\mu\text{A}/\text{cm}^2$ to prevent significant overheating of the substrate relative to room temperature (the overheating did not exceed 50°C). Next, isochronous annealing was performed for 1 h under an oxygen flow in a quartz tube at temperatures from 400 to 1000°C with an increment of 100°C.

After annealing at the temperature optimal for obtaining the ZnO phase (about 700°C), the samples were irradiated with fast ¹³²Xe²⁶⁺ ions at an angle of 45° to the surface of the SiO₂ film with an energy of 167 MeV in the range of fluences from 1×10^{12} to $5 \times 10^{14} \text{ cm}^{-2}$. Irradiation was carried out at the ITs–100 cyclotron of the Laboratory of Nuclear Reactions, Joint Institute for Nuclear Research. A homogeneous—with an accuracy of up to 5%—distribution of particles over the surface of the target was achieved by scanning the beam in the vertical and horizontal directions. The ion flux density was $2 \times 10^9 \text{ (cm}^2 \text{ s)}^{-1}$. The temperature of the samples during irradiation did not exceed 30°C.

The surface topography of the samples was studied using the method of scanning electron microscopy (SEM) in a TESCAN LYRA3 microscope operating in the modes of secondary electron emission (topological contrast) and the elastic backscattering of electrons (*Z*-contrast). The microscope was equipped with an attachment for energy dispersive spectroscopy.

The sample surfaces were also visualized using an MFP-3D scanning probe microscope (Asylum Research) operating in the semi-contact mode, as well

Table 1. Data of energy dispersive analysis of the sample after implanting with Zn ions

Element	Concentration, wt %	Concentration, at %
C	27.93	43.17
O	18.56	21.53
Si	53.32	35.25
Zn	0.19	0.05
Total	100.00	100.00

as in the Kelvin probe mode using an NSG30/Pt (Tipsnano) cantilever with a hardness of 25 N/m and a resonant frequency of free vibrations of 330 kHz. The obtained images were processed using Gwyddion software.

The photoluminescence (PL) spectra were recorded at 10 K in the wavelength range of 350–620 nm using a He–Cd laser with a wavelength of 325 nm for optical pumping. We also studied the reflection spectra in the wavelength range of 400–800 nm and the light reflection spectra in the same range for two mutually perpendicular directions of polarization of the incident light.

RESULTS AND DISCUSSION

Surface Studies in a Scanning Electron Microscope

According to the SEM data, individual micrometer-sized particles are visualized after implantation of Zn ions, which are hydrocarbon contaminants, since they contain elements lighter than the elements of the matrix, i.e., Si and O, and the Zn impurity. The energy dispersive spectrum of the surface beyond the observed particles consists of lines corresponding to elements of the oxide film, i.e., Si and O, implanted Zn, and C contaminants. The results of energy dispersive microanalysis of the surface are given in Table 1. It should be noted that contamination with hydrocarbons is caused by insufficient purification of the atmosphere of the vacuum chamber from oil vapor, since an oil pump is used to evacuate air from the working chamber.

A SEM image of the surface of a SiO₂ film after annealing for 1 h in an O₂ stream at a temperature of 700°C is shown in Fig. 1. A large bright particle about 1 micron in size is seen in the image of the SiO₂-film surface (Fig. 1a), which is obtained in the mode of detection of secondary electron emission (topological contrast). In Fig. 1b, an image of the same particle was obtained in the mode of backscattered electron detection (*Z*-contrast). In the latter image, it is brighter than the surrounding background. This indicates that its composition includes elements that are heavier than Si and O. The energy dispersive spectrum of this particle is shown in Fig. 2, from which it follows that it consists of several elements. Their concentrations are given in

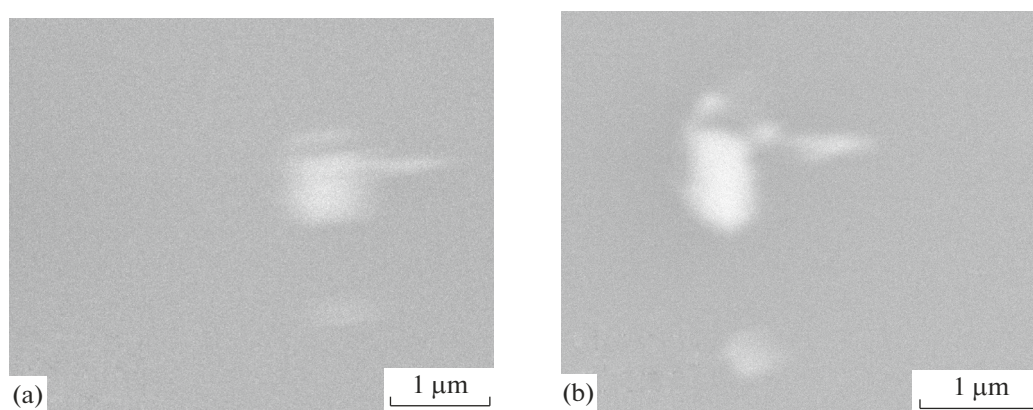


Fig. 1. SEM images of the sample surface after annealing at 700°C that are obtained in the modes of detecting the emission of (a) secondary electrons and (b) backscattered electrons.

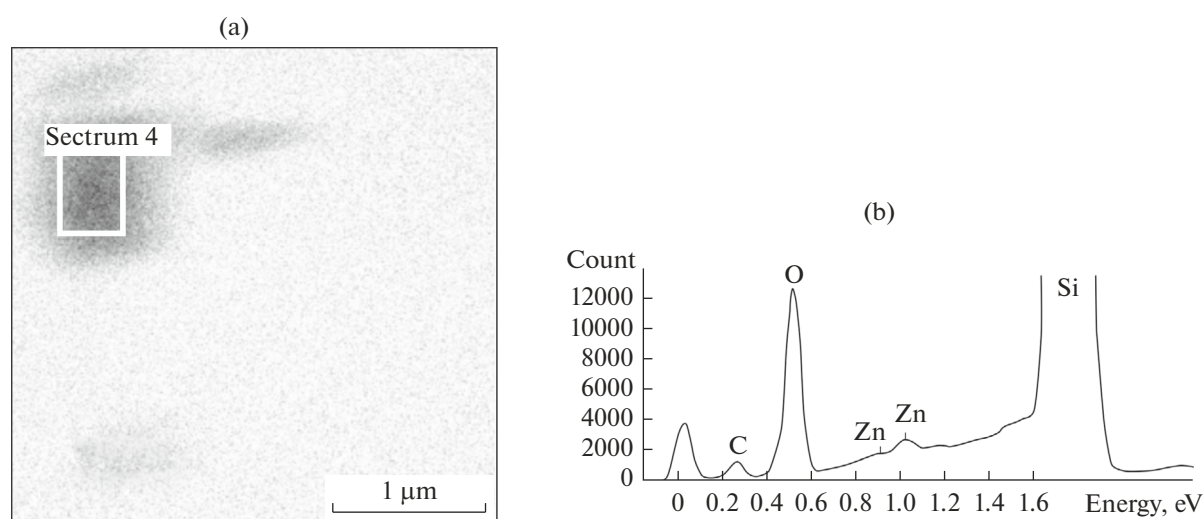


Fig. 2. (a) SEM image of a particle that is obtained in the mode of detecting the emission of secondary electrons and (b) the energy-dispersive spectrum from the frame shown in part (a).

Table 2. In addition to the elements of the oxide film, i.e., Si and O, and implanted Zn, and C contaminants are also detected. Thus, it becomes clear that the visualized particle contains Zn. Investigation of the background near the bright particle showed that the energy dispersive spectrum complies, with an accuracy of 0.1 at %, with the data given in Table 2. It is obvious that the bright particle in Fig. 1 contains Zn. These can be either particles of zinc itself or its oxide compounds, for example, ZnO or Zn₂SiO₄, which is less often formed at this annealing temperature. It is also possible that the particle represents a mixture.

Two SEM images of the surface after irradiation with fast Xe ions with a fluence of $5 \times 10^{14} \text{ cm}^{-2}$ are shown in Fig. 3. One can see light spots about 1 μm in size in Fig. 3a (topological contrast), which are small pits on the surface of the SiO₂ film. These pits appear to be related to radiation effects caused by irradiation

with fast Xe ions. Comparison of these spots with the image in Fig. 3b shows that they have a lighter shade compared to the general background, i.e., the pits are filled with elements that are lighter than the elements

Table 2. Data of energy dispersive analysis of the sample after annealing at 700°C

Element	Concentration, wt %	Concentration, at %
C	7.82	14.43
O	21.54	29.87
Si	70.42	55.62
Zn	0.22	0.08
Total	100.00	100.00

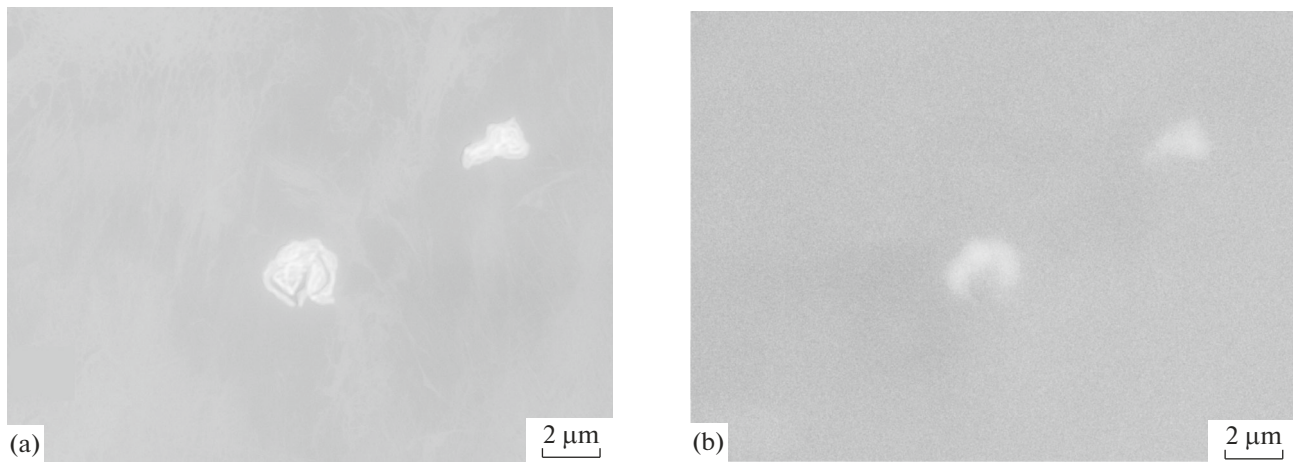


Fig. 3. SEM images of the sample surface after irradiation with Xe ions at a fluence of $5 \times 10^{14} \text{ cm}^{-2}$ that are obtained in the modes of detecting the emission of (a) secondary electrons and (b) backscattered electrons.

of the matrix, e.g., Si and O. Most likely, these are hydrocarbon contaminants.

Analysis of the Surface Topology in an Atomic Force Microscope

Two- and three-dimensional images of the silicon surface after the implantation of Zn are given in Fig. 4a. A statistical analysis of the AFM images showed that the SiO_2 sample implanted with Zn atoms is characterized by the highest roughness parameters, namely: $R_{\text{ms}} = 860 \text{ pm}$ and $R_{\text{a}} = 680 \text{ pm}$. For the sample after annealing in an O_2 atmosphere, $R_{\text{ms}} = 155 \text{ pm}$ and $R_{\text{a}} = 123 \text{ pm}$. Finally, the lowest values were obtained for the sample irradiated with Xe ions, namely: $R_{\text{ms}} = 127 \text{ pm}$ and $R_{\text{a}} = 98 \text{ pm}$.

The surface is characterized by the following parameters: the average value of the heterogeneity is $R_{\text{a}} = 680 \text{ pm}$; the average roughness is $R_{\text{a}} = 0.680 \text{ nm}$; and its root-mean-square value is $R_{\text{ms}} = 860 \text{ pm}$. Two- and three-dimensional images of the surface after annealing at 700°C are shown in Fig. 4b. The surface is characterized by the following parameters: the average roughness is $R_{\text{a}} = 123 \text{ pm}$ and its root-mean-square value is $R_{\text{ms}} = 155 \text{ pm}$. After irradiation with Xe ions at a fluence of $5 \times 10^{14} \text{ cm}^{-2}$ (Fig. 4c), the smallest roughness values are observed, namely: the average value is $R_{\text{a}} = 98 \text{ pm}$ and its root-mean-square value is $R_{\text{ms}} = 127 \text{ pm}$. It should be noted that the surface is rather homogeneous after implantation. However, nanoparticles with a cross-sectional size of 20–50 nm and an average height of about 1–5 nm are formed on it after annealing at 700°C . Such surface structuring can be associated with the diffusion of zinc to the surface of the sample and the formation of its clusters in the subsurface layer, in which precipitates of its oxides or silicides are formed.

A topographic AFM image of the sample surface after annealing in an oxygen atmosphere at 400°C and a potential image (Kelvin probe mode) are shown in Fig. 5. As can be seen from the comparison of these two images, bright spots (protuberances) (Fig. 5a) are transformed into areas with a lower negative potential (Fig. 5b). This indicates the metallic nature of these protuberances. As noted above, zinc is a rapidly diffusing impurity; therefore, it can appear on the surface of a silica film by diffusion to the surface, which is an unlimited drain for impurities. The situation gets even worse if we examine such a sample after annealing at 600°C . The reverse diffusion of zinc from the sample increases and large agglomerates of Zn-containing compounds are already visible on the surface (Fig. 6a). In Fig. 6b, a large Zn-containing agglomerate in the center of the image is characterized by a lower value of the potential. It should be noted that an increase in the potential is observed around this agglomerate.

Nanoparticle Size

It is known that nanoparticles should be synthesized in a narrow size range when creating emitting components based on the ZnO phase; in that case, the width of the emission line of exciton luminescence is narrowed. In [16], a new method was proposed to selectively change and control the size of formed metal nanoparticles by irradiating a substrate with beams of fast heavy ions. This kind of irradiation leads to the formation of deformation latent tracks (disordered nanometer-sized regions around the trajectory of the irradiating ion) in many crystals. The corresponding irradiation that creates the track can change the nanoparticle shape from spherical to ellipsoidal. This effect is most noticeable with numerous actions (about 100 times) exerted by fast heavy ions [17].

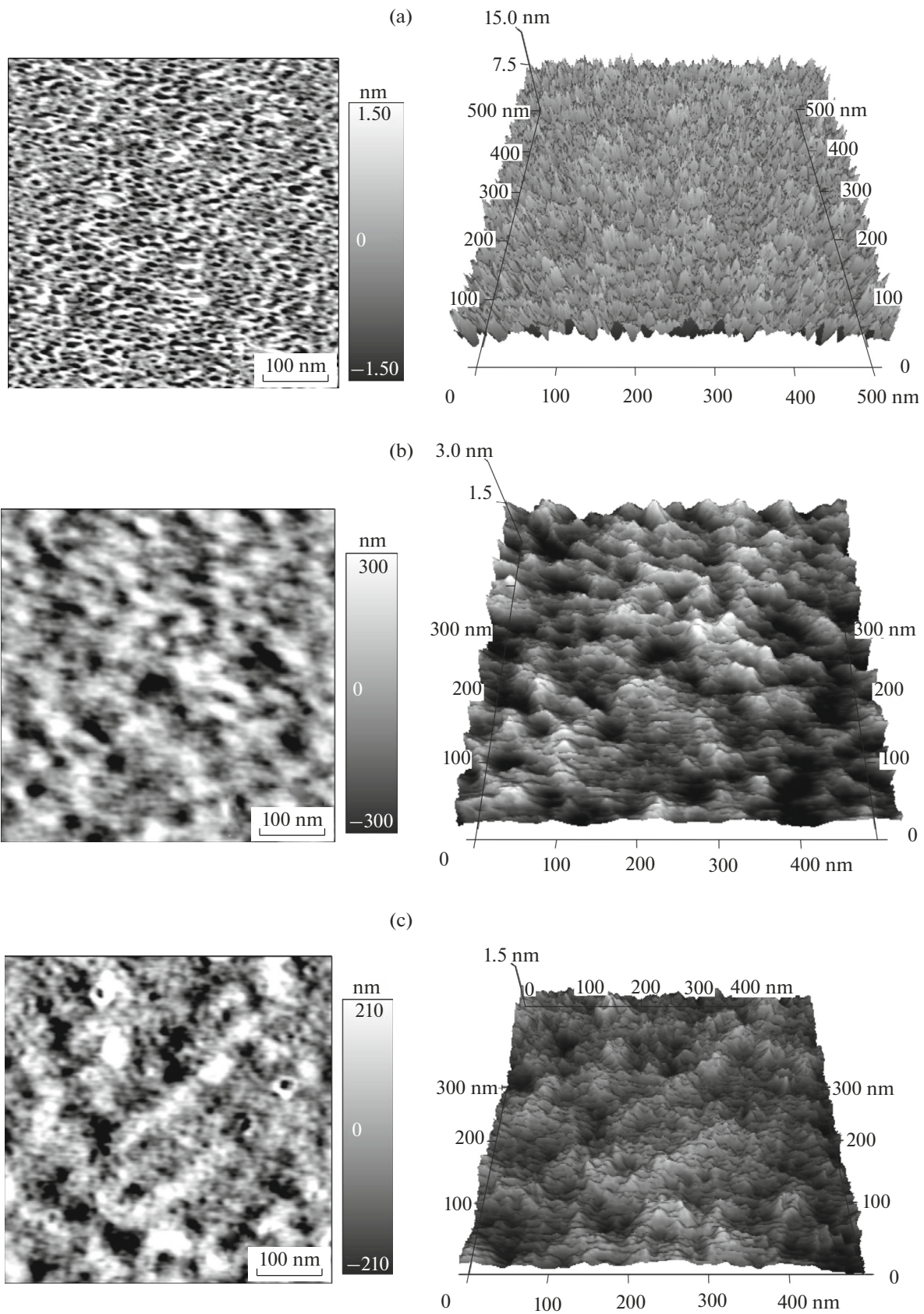


Fig. 4. Two-dimensional (on the left) and three-dimensional (on the right) AFM images of the sample surface (a) after the implantation of Zn, (b) after annealing at 700°C in an O₂ atmosphere, and (c) after irradiation with Xe ions at a fluence of $5 \times 10^{14} \text{ cm}^{-2}$.

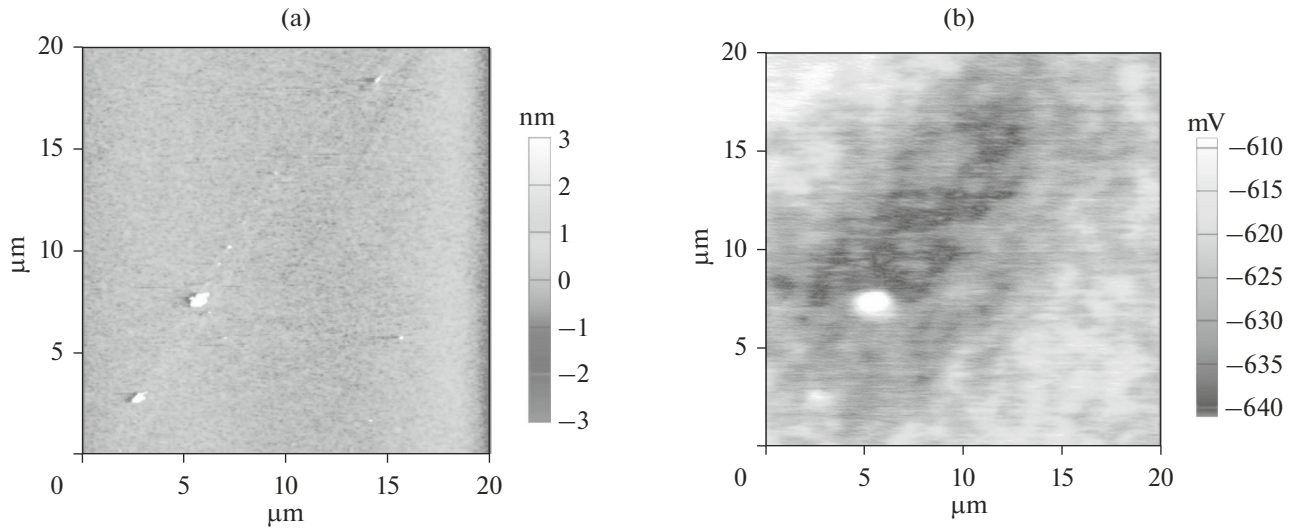


Fig. 5. (a) Surface topography and (b) potential of the sample after annealing at 400°C.

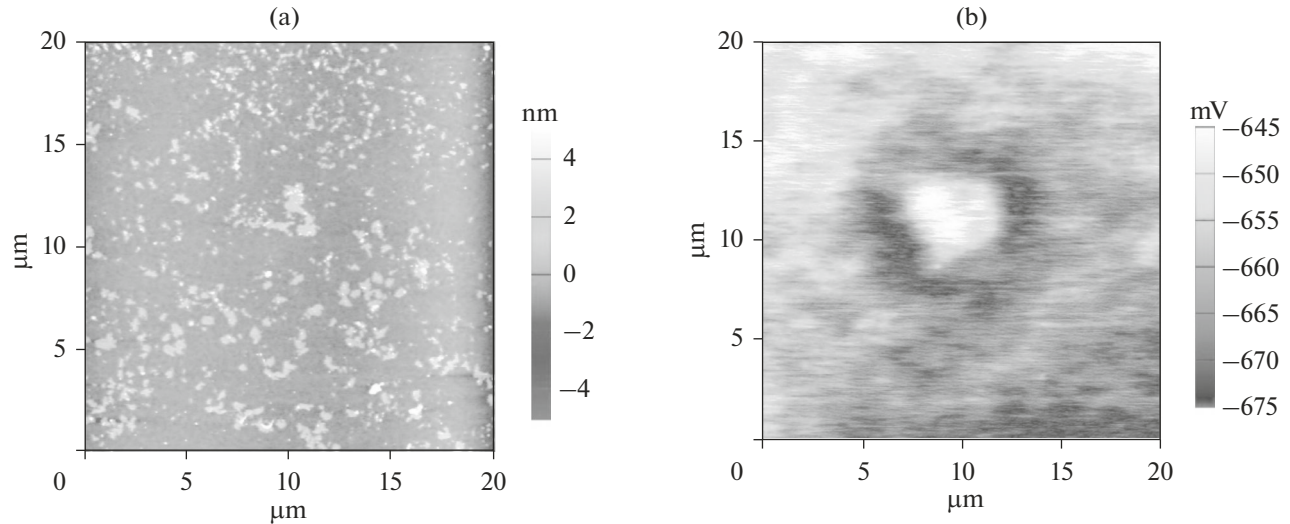


Fig. 6. (a) Surface topography and (b) potential of the sample after annealing at 600°C.

After annealing in an O_2 atmosphere at a temperature of about 700°C, the samples were irradiated with fast $^{132}\text{Xe}^{26+}$ ions at an energy of 167 MeV in the fluence range from 1×10^{12} to $5 \times 10^{14} \text{ cm}^{-2}$ in order to modify the synthesized zinc-oxide nanoparticles. The parameters of ions passing through the amorphous SiO_2 film were calculated using the SRIM 2013 software package [18] and were as follows: the energy loss in the electron system is $dE_{\text{el}}/dx = 14.7 \text{ keV/nm}$; the energy loss in the nuclear system is $dE_{\text{nucl}}/dx = 59.8 \text{ eV/nm}$; the projective path is $R_p = 18.6 \text{ }\mu\text{m}$; the longitudinal straggling is $S_{\text{tr}} = 0.576 \text{ }\mu\text{m}$; and the lateral straggling is $S_{\text{lat}} = 0.622 \text{ }\mu\text{m}$.

As was shown in [19] by the method of small-angle scattering, the radius of the track of Xe ions in amorphous SiO_2 is a function of the energy loss in the electron system (dE_{el}/dx). In the case of Xe ions with an energy of 167 MeV, the energy loss in the electron system of the SiO_2 matrix is 14.7 keV/nm, which corresponds to a track radius of $r \approx 4 \text{ nm}$. In the mentioned work, an important quantity for estimating the influence of ion tracks on the irradiated surface was also introduced, namely, the coverage ratio $CR = \pi r^2 \Phi$, where Φ is the fluence of fast ions. The coverage ratio shows how many times the average surface is crossed by ion tracks. In the present study, this parameter equals 0.5–250 in the range of fluences between 1×10^{12} and

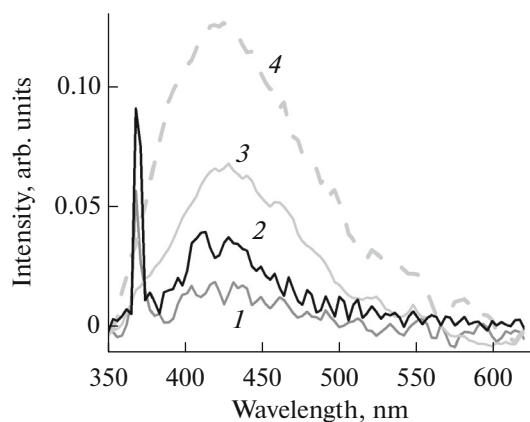


Fig. 7. PL spectra of the SiO₂ film (1) implanted with Zn, (2) annealed in an oxygen atmosphere at 700°C, and irradiated with fast Xe ions at fluences of (3) 2×10^{13} and (4) 5×10^{14} cm⁻². The PL spectra were recorded at a temperature of 10 K.

5×10^{14} cm⁻². As was mentioned above, the *CR* value should be greater than 100 for a significant change in the shape of nanoparticles.

When nanoparticles are exposed to fast heavy ions, the maximum size of nanoparticles that melt upon irradiation plays an important role. In the case of irradiation with Xe ions at an energy of 167 MeV, the maximum size $R_{\text{NP}}^{\text{max}}$ of zinc-oxide nanoparticles is defined as follows [17]:

$$R_{\text{NP}}^{\text{max}} = \sqrt{\frac{3(dE/dx)_{e,\text{NP}}}{2\pi(H_{\text{NP}}^m \rho_{\text{NP}} + Q)}}$$

where the specific energy loss of the Xe ion for electronic excitations in zinc oxide nanoparticles is $(dE_{\text{el}}/dx)_{e,\text{NP}} = 25.9$ keV nm⁻¹, the specific melting heat of zinc oxide is $= 694$ J/g, and the density of zinc oxide is $\rho_{\text{NP}} = 5.61$ g/cm³. Here, Q is the heat, which is spent heating the zinc-oxide nanoparticles to the melting point and determined from relation $Q = \rho_{\text{NP}} c (T_m - T_{\text{irr}})$, where the specific heat equals $c = 0.495$ J/(g K), the melting point of zinc oxide is $T_m = 1975^\circ\text{C}$, and the temperature of the sample during irradiation is $T_{\text{irr}} = 20^\circ\text{C}$. Substituting all of the above values into the formula for determining Q , we find that $Q = 5430$ J/cm⁻³ and, eventually, $R_{\text{NP}}^{\text{max}} = 14.6$ nm.

It should be noted that the above calculations are estimates. As was shown in [20], the Gibbs heat for the reaction $2\text{ZnO} \rightarrow 2\text{Zn} + \text{O}_2$ is $\Delta G(T) = +350$ kJ/mol at 300 K. In other words, this reaction does not proceed spontaneously at room temperature. However, the Gibbs heat of this reaction becomes negative upon a significant increase in the temperature, for example, up to 2350°C, and the reaction of decomposition of

zinc oxide to Zn and O₂ can proceed spontaneously as a result.

Study of the Photoluminescence Spectra

The PL spectra of the samples after Zn implantation, after annealing at 700°C, and after irradiation with fast Xe ions at different fluences are shown Fig. 7. One can see that a narrow PL peak associated with the formation of the ZnO phase and exciton recombination in it appears at a wavelength of 370 nm after Zn implantation (curve 1) against the background of a broadened peak with a center near 420–430 nm, which is attributable to the arisen radiation point defects and their clusters. This peak increases after annealing at 700°C (curve 2), since oxygen molecules diffusing into the sample from the surrounding atmosphere reach the implanted zinc ($R_p = 40$ nm), oxidize it, and thereby increase the total content of the zinc-oxide phase in the sample during the process of annealing in an oxidizing atmosphere. After irradiation of the sample with fast Xe ions at a fluence of 5×10^{12} cm⁻², the PL peak at 370 nm practically disappears, which may indicate a decrease in the content of the ZnO phase in the film under study. At the same time, the broadened PL peak with a center at 425 nm increases significantly with an increase in the fluence of Xe to 5×10^{14} cm⁻².

Study of the Reflection Spectra

It is known [21] that a layer transparent in the visible region of the spectrum, such as a dielectric SiO₂ film, changes its transparency and reflection spectrum upon the implantation of large concentrations of metal impurities. In particular, absorption increases due to surface plasmon resonance and reflection also behaves in a similar way. For correct interpretation, the reflection spectra were represented as the ratio of the measured reflection spectrum to the spectrum of the initial SiO₂ film deposited onto the Si substrate, before being implanted with zinc. The results are given in Fig. 8. As the annealing process advances, the metallic zinc phase is transformed into the phase of its oxide and the sample becomes transparent.

As is known, the maximum distribution of implanted Zn under the given conditions of implantation is at a depth of 40 nm, which corresponds to the R_p value calculated using the SRIM software package. Precipitates of zinc are also located here, since its content significantly exceeds the limit of its equilibrium solubility in silicon oxide. The spread of the concentration of implanted zinc and the position of its maximum also correspond to the values calculated using the SRIM software package. Since the obtained concentrations of Zn significantly exceed its limiting equilibrium solubility in silicon oxide, Zn can precipitate near the concentration maxima in the form of

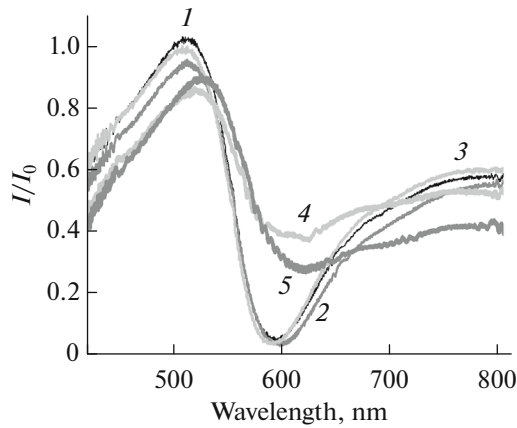


Fig. 8. Normalized reflection curves (I) after implantation, and after annealing at (2) 400, (3) 600, (4) 700, and (5) 800°C.

implanted metallic Zn and/or its oxide compounds like $\text{ZnO} \cdot \text{ZnSiO}_3$ after annealing at temperatures below 700°C or $\text{ZnO} \cdot \text{Zn}_2\text{SiO}_4$ at higher annealing temperatures (above 800°C).

Upon heat treatment in an oxygen atmosphere in the temperature range of 600–900°C, radiation-induced defects are gradually annealed. At temperatures above 600°C, the diffusion coefficient of zinc in silicon oxide significantly increases [22]. The high diffusion mobility of zinc contributes to its active redistribution in the area of the implanted layer. After annealing at 900°C, the defects are almost completely annealed and the content of zinc in the sample noticeably decreases, since its smaller part has diffused to the depth of the substrate and the larger part has exhausted from the sample into the atmosphere as a result of reverse diffusion.

CONCLUSIONS

A ZnO phase and a characteristic PL peak at a wavelength of 370 nm are detected after the implantation of Zn into a silicon-oxide film. Low-temperature annealing in the temperature range of 400–600°C leads to the formation of a SiO_2 film and Zn-containing precipitates with a cross-sectional size of about 100 nm on its surface. After annealing in the temperature range of 700–800°C, Zn-containing precipitates of the chemical composition $\text{Zn} \cdot \text{ZnO}$ are formed in the film, and a phase with chemical composition $\text{ZnO} \cdot \text{Zn}_2\text{SiO}_4$ is formed after annealing at temperatures of 900–1000°C.

According to the AFM data, the initial SiO_2 sample implanted with Zn is characterized by the largest parameters of roughness, namely: $R_{\text{ms}} = 860$ pm and $R_a = 680$ pm. After annealing in an O_2 atmosphere at

700°C, $R_{\text{ms}} = 155$ pm and $R_a = 123$ pm. The surface of the sample irradiated with Xe ions at a fluence of $5 \times 10^{14} \text{ cm}^{-2}$ has the smallest parameters of roughness, specifically: $R_{\text{ms}} = 127$ pm and $R_a = 98$ pm.

Irradiation with fast Xe ions leads to, on the one hand, destruction of the ZnO phase, which confirms the disappearance of the exciton PL peak at a wavelength of 370 nm, and on the other hand, the formation of a large number of radiation defects and characteristic luminescence with a maximum at 430 nm, which increases with an increase in the radiation intensity. After irradiation with Xe, shallow pits of micrometer dimensions in the image plane are detected on the surface of the SiO_2 film.

ACKNOWLEDGMENTS

This work was carried out in part within the State Assignment of the Federal Agency of Scientific Organizations of the Russian Federation (state project no. 14, topic 40.3, section no. 0066-2014-0025, and topic 40.2, section no. 0066-2014-0024), and in part within the State Assignment for the Institute of Physics and Technology, Russian Academy of Sciences. Studies involving the methods of scanning probe microscopy were carried out under financial support of the Ministry of Science and Higher Education of the Russian Federation using equipment of the Center for Collective Use Materials Science and Metallurgy of the National Research University of Science and Technology MISiS (state assignment no. 11.9706.2017/7.8).

REFERENCES

1. C. W. Litton, T. C. Collins, and D. S. Reynolds, *Zinc Oxide Material for Electronic and Optoelectronic Device Application* (Wiley, Chichester, 2011).
2. H. Amekura, Y. Sakuma, K. Kono, et al., *Phys. B (Amsterdam, Neth.)* **376–377**, 760 (2006).
3. C. Y. Jiang, X. W. Sun, G. Q. Lo, et al., *Appl. Phys. Lett.* **90**, 263501 (2007).
4. C. Li, Y. Yang, X. W. Sun, et al., *Nanotechnology* **18**, 135604 (2007).
5. S. Chu, M. Olmedo, Zh. Yang, et al., *Appl. Phys. Lett.* **93**, 181106 (2008).
6. G. P. Smestad and M. Gratzel, *J. Chem. Educ.* **75**, 752 (1998).
7. D. M. Bagnall, Y. F. Chen, M. Y. Shen, et al., *J. Cryst. Growth* **184–185**, 605 (1998).
8. J. S. Dodds, F. N. Meyers, and K. J. Loh, *Smart Struct. Syst.* **12**, 055 (2013).
9. H. Chang, H. D. Park, K. S. Sohn, and J. D. Lee, *J. Korean Phys. Soc.* **34**, 545 (1999).
10. B. B. Straumal, A. A. Mazilkin, S. G. Protasova, et al., *Phys. Rev. B* **79**, 205206 (2009).

11. D.-I. Son, D.-H. Park, W. K. Choi, et al., *Nanotechnology* **20**, 195203 (2009).
12. V. Privezentsev, V. Kulikauskas, E. Steinman, and A. Bazhenov, *Phys. Status Solidi C* **10**, 48 (2013).
13. H. Amekura, Y. Takeda, and N. Kishimoto, *Mater. Lett.* **222**, 96 (2011).
14. Y. Y. Shen, X. D. Zhang, D. C. Zhang, et al., *Mater. Lett.* **65**, 2966 (2011).
15. V. V. Privezentsev, N. Yu. Tabachkova, K. B. Eidelman, and S. V. Ksenich, *Bull. Russ. Acad. Sci.: Phys.* **80**, 1421 (2016).
16. C. D'Orleans, J. Stoquert, C. Estourne's, et al., *Phys. Rev. B* **67**, 220101 (2003).
17. F. F. Komarov, O. A. Milchanin, V. A. Skuratov, et al., *Bull. Russ. Acad. Sci.: Phys.* **80**, 160 (2016).
18. J. F. Ziegler, and J. P. Biersack, SRIM 2013. <http://www.srim.org>.
19. P. Kluth, C. S. Schnohr, O. H. Pakarinen, et al., *Phys. Rev. Lett.* **101**, 175503 (2008).
20. L. P. Vladimirov, *Thermodynamic Calculations for Equilibrium of Metallurgical Reactions* (Metallurgiya, Moscow, 1970) [in Russian].
21. D. Zatsepin, A. Zatsepin, D. Boukhvalov, et al., *J. Non-Cryst. Solids* **432**, 183 (2016).
22. *Diffusion in Condensed Matter: Methods, Materials, Models*, Ed. by P. Heitjans and J. Kärger (Springer, 2005), **Vols. 376–377**, p. 760.

Translated by O. Kadkin